THE JOURNAL OF PHYSICAL CHEMISTRY C

Article

pubs.acs.org/JPCC

Effects of Axial Coordination of the Metal Center on the Activity of Iron Tetraphenylporphyrin as a Nonprecious Catalyst for Oxygen Reduction

Jerzy Chlistunoff* and Jose-Maria Sansiñena

Los Alamos National Laboratory P.O. Box 1663, Los Alamos, New Mexico 87545, United States

Supporting Information

ABSTRACT: Effects of axial coordination of the metal center on oxygen reduction catalyzed by iron tetraphenylporphyrin have been studied using spectroelectrochemical and rotating ring disk electrode techniques. Among numerous ligands studied, the strongest complexation of the metal center was observed for imidazole and some substituted imidazole ligands. Around 300 mV positive shift of the oxygen reduction potential in 0.5 M H_2SO_4 was observed when the catalyst support (high surface area carbon Vulcan XC72) was impregnated with polyvinylimidazole. A smaller 200 mV shift of the reduction potential was recorded when graphene modified with 1-(3-aminopropyl)imidazole was used as the catalyst support instead of Vulcan. In both cases, the catalyst selectivity for four-electron reduction was also substantially improved. The effects of iron complexation on oxygen reduction kinetics and mechanism result from both a positive shift of the potential of the first porphyrin reduction and an increase of the electron density on the iron center through the so-called "push effect". The observed phenomena are discussed in relation to heat-treated Fe/N/C catalysts for oxygen reduction.

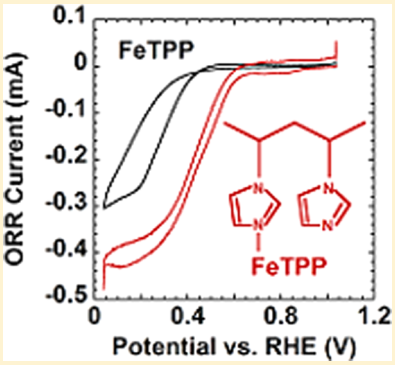

INTRODUCTION

One of the few remaining barriers for polymer electrolyte fuel cells (PEFC) to become power sources for automotive transportation is the shortage of a suitable cathode catalyst. Platinum-based catalysts seem to be close to meet both activity and durability criteria,[1] but the global resources of Pt are not only limited but also monopolized to a large extent. A variety of alternative materials that could possibly replace platinum as an oxygen reduction reaction (ORR) catalyst have been explored. The most promising among them are materials obtained by pyrolysis of suitable iron, nitrogen, and carbon precursors (Fe/N/C catalysts). In terms of active site turnover frequencies, their activity approaches that of platinum.[2,3] However, the volume activities of such materials frequently suffer from insufficient densities of the active sites, obstructed access to them,[4,5] and also significant Tafel slopes at higher overpotentials.[6] Pyrolyzed catalysts are rather complex materials, and there still exist controversies regarding the nature of their active sites. A majority of the scientific community, including the authors of this paper, tend to believe that iron is an important part of the active site in such catalysts. Recent studies indicate that the iron atoms are coordinated by four nitrogens in a square planar arrangement, where the nitrogen atoms belong to pyridine rings embedded in graphene planes.[7,8]

Oxygen reduction is part of numerous biological cycles and accomplished through enzymatic catalysis. As these natural processes are not constrained by any artificial boundaries, the problem of a limited space and thus of insufficient active site density does not exist. Consequently, very bulky molecules are frequently involved in biological catalysis. Such molecules cannot be used in many man-created applications. For instance, copper laccase would likely outperform platinum[9] as an ORR catalyst, if it was not for the size of the laccase molecule, which prevents achieving a required active site density for PEFC applications. Moreover, the most advanced PEFCs utilize highly acidic polymer electrolytes, which would be deadly for the enzyme. That copper laccase cannot be used in man-created applications does not mean that useful hints cannot be obtained from natural processes in an attempt to create an effective catalyst for ORR. Macrocyclic complexes of transition metals, frequent building blocks of enzymatic catalysts, were explored as potential oxygen reduction catalysts as early as in 1964.[10] Later, a discovery was made that pyrolysis of the macrocycles may result in materials that exhibit even higher activity.[11,12] This was the beginning of pyrolyzed Fe/N/C catalysts. Despite the advent of the Fe/N/C materials, numerous articles on porphyrins and other macrocyclic compounds as potential ORR catalysts have been published to date. Among them, papers from Anson's group played a pivotal role in that field.[13,14] It is well known that in biological systems in addition to macrocyclic compounds other molecules actively participate in oxygen activation, reduction, and transport. For instance, ubiquinone (coenzyme Q10) acts as an electron shuttle in citric acid cycle.[15] On the other hand, axial anionic ligands, e.g., imidazolate in peroxidase, phenolate in catalase, and thiolate in cytochrome P-450, are regarded as essential agents to aid the

Received: May 5, 2014
Revised: July 31, 2014
Published: August 1, 2014

   dx.doi.org/10.1021/jp5044249 | J. Phys. Chem. C 2014, 118, 19139−19149

heterolytic O−O bond cleavage. They are believed to be responsible for the so-called "push effect", where the axial ligands act as strong internal electron donors.[16−20] There are also examples where proximal functional groups exert a beneficial effect on ORR catalyzed by metal macrocycles, e.g., acidic groups such as carboxyl[22] or even protonated pyridyl[23] acting as proton shuttles in ORR catalyzed by iron macrocycles. As the above examples illustrate, bringing together macrocyclic complexes of metals and suitable functional groups can promote a more effective ORR catalysis than that supported by the sole macrocyclic complexes. In this paper we show that the activity and selectivity of iron tetraphenylporphyrinate as an oxygen reduction catalyst can be greatly improved by axial complexation of the metal center by imidazoles. Quantum mechanical calculations by Tsuda and Kasai[24] also predicted an enhancement of ORR through axial complexation of metalloporphyrins by imidazoles. Similarly, polyvinylpyridine was reported to improve the kinetics of ORR catalyzed by a cobalt phthalocyanine in acidic media,[25] whereas iron phthalocyanine anchored through an axial pyridinic ligand to carbon nanotubes was demonstrated to outperform Pt as an ORR catalyst in alkaline solutions.[26]

EXPERIMENTAL SECTION

Imidazole (ACS reagent, ≥99%, Sigma-Aldrich), 1-(3-aminopropyl)imidazole (≥97%, Aldrich), 1-butylimidazole (98%, Aldrich), 1-(diethoxymethyl)imidazole (≥97%, Aldrich), 1-methylimidazole (ReagentPlus, 99%, Aldrich), 2-methylimidazole (99%, Aldrich), cyclohexylamine (ReagentPlus, 99%, Aldrich), and pyridine (spectrophotometric grade, ≥99%, Sigma-Aldrich) were used as received. Iron(III) tetraphenylporphyrin chloride (5,10,15,20-tetraphenyl-21*H*,23*H*-porphine iron(III) chloride), hereafter called FeTPPCl, was HPLC grade (>94%, Aldrich) and used as received. HPLC-grade dichloromethane (≥99.9% with 50−150 ppm amylene as stabilizer, Sigma-Aldrich) and ACS spectrophotometric-grade acetone (≥99.5%, Sigma-Aldrich) were used as solvents for spectrophotometry/spectroelectrochemistry. Reduced graphene oxide with covalently linked piperazine (RGO-NH, NanoInnova Technologies, Spain) and reduced graphene oxide with covalently linked 2,2′-(ethylenedioxy)bis(ethylamine) (RGO-NH2, NanoInnova Technologies, Spain) were used as received. Vulcan XC72, a high surface area (~400 $m^2\ g^{-1}$) carbon (Cabot), was used as received.

Synthesis of polyvinylimidazole (PVI) for the most part followed the method published by Savin et al.[27] A 10 g sample of 1-vinylimidazole (Aldrich) was dissolved in 16.5 cm^3 of toluene (ACS reagent, ≥99.5%, Sigma-Aldrich) and poured into a round-bottom flask. The solution was heated under argon up to 70 °C. Subsequently, 2.5 g of the polymerization initiator, 2,2′-azobis(isobutyronitrile) (AIBN), was added to the flask, and the reaction mixture was vigorously stirred under Ar at 70 °C. A yellowish PVI deposit quickly precipitated, but stirring continued for 2 h. After reaction, PVI was separated by vacuum filtration and purified two times through dissolution in methanol followed by reprecipitation with acetone and dried at 70 °C overnight. On the basis of previous work,[27,28] the molecular mass of the product is around $(1−2) \times 10^5$ g mol^{-1}.

One-pot synthesis of reduced graphene oxide with covalently linked 3-aminopropylimidazole (G-IMD) was performed according to a published procedure[29] using two times smaller quantities of the reagents compared to the original work.

Spectrophotometric measurements were performed at ambient conditions using a Hewlett-Packard model 8452A diode array spectrophotometer and 1 cm quartz cuvettes. The same instrument was used in spectroelectrochemical studies.

A quartz spectroelectrochemical cell with 0.5 mm optical path (Bioanalytical Systems, Inc.) equipped with a fine Au mesh as the working electrode, Pt wire as the counter electrode, and a Vycor frit separated silver wire as the quasi reference electrode (AgQRE) were used for all spectroelectrochemical experiments. In accordance with literature data,[30] the potential of the AgQRE in pure electrolyte solution was found to be stable and reproducible. The electrolyte was 0.1 mol dm^{-3} $TBAPF_6$ (Fluka, electrochemical grade) in dichloromethane (DCM).

All voltammetric experiments utilizing DCM as a solvent were performed under ambient conditions using 0.1 mol dm^{-3} $TBAPF_6$ as the electrolyte and a 100 μm platinum microelectrode (Bioanalytical Systems) as the working electrode. The counter electrode in those experiments was a platinum mesh, and AgQRE served as the reference. For both spectroelectrochemical and voltammetric experiments, the potentials quoted in the paper are referenced vs ferrocene, which was used as an internal standard. Solutions were either deoxygenated or oxygenated by purging oxygen or ultra-high-purity argon. Before entering the cell, the gases were first saturated with DCM vapor in two bubblers equipped with gas dispersion tubes and filled with 0.1 mol dm^{-3} $TBAPF_6$ solution in DCM.

All RRDE experiments were performed using 0.5 mol dm^{-3} H_2SO_4 at 25 °C using a jacketed glass cell. The working electrode was a Pine model AFE7R9GCPT electrode with a glassy carbon disk and a platinum ring. Its nominal collection efficiency of 37% was confirmed by independent measurement using potassium ferricyanide in potassium chloride electrolyte solutions. The counter electrode was a graphite rod, whereas the reference electrode was a hydrogen electrode utilizing 6% H_2 in Ar in equilibrium with Pt black-coated platinum wire immersed in 0.5 mol dm^{-3} H_2SO_4. The equilibrium potential of the reference electrode at Los Alamos elevation (2100 m) is 39 mV positive than the potential of the RHE in this solution.

A Princeton Applied Research potentiostat model 283 controlled by Corrware software (Scribner Associates) was used for all spectroelectrochemical and voltammetric experiments involving DCM as a solvent. A Pine Instruments bipotentiostat model AFCBP1 controlled by Aftermath software (Pine Instruments) was used for all rotating ring disk experiments.

With one exception, all catalyst inks for RRDE experiments were prepared using a single procedure. Around 20 mg of a carbonaceous catalyst support (Vulcan XC72, RGO-NH, RGO-NH2, G-IMD) was mixed with ~4 mg of FeTPPCl and ~2 cm^3 of DCM and sonicated to dryness. Afterward, the dry residue was sonicated with 5 cm^3 of isopropanol and 30 μL of 5% Nafion solution (Ion Power) until a uniform suspension was obtained. For PVI containing inks, the Vulcan XC72 carbon support (~20 mg) was first impregnated with PVI through sonication of ~5 cm^3 of a methanol solution containing 4−5 mg of PVI until a dry residue was obtained. Subsequent ink preparations followed the procedure used for non PVI inks (see above) except the impregnated XC72 was used instead of the pure material. Typically, a 20 μL volume of the ink was deposited onto the RRDE disk for measurements.

dx.doi.org/10.1021/jp5044249 | J. Phys. Chem. C 2014, 118, 19139−19149

AXIAL COORDINATION OF FETPPCL BY DIFFERENT LIGANDS

UV−vis spectrophotometry was selected as a method for studying reactions between FeTPPCl and potential axial ligands. Since iron tetraphenylporphyrin chloride (FeTPPCl) is insoluble in water, reactions were studied using solvents which guaranteed sufficient solubility of both the porphyrin and the ligands. Dichloromethane (DCM) was found to be a suitable solvent for reactions involving the following ligands containing aromatic nitrogen (pyridine, unsubstituted and substituted imidazoles), aliphatic nitrogen (cyclohexyloamine, aniline), pyrrolic nitrogen (pyrrole), as well as aromatic (tiophene) and aliphatic (2-mercaptobenzimidazole) sulfur.

No meaningful complexation of FeTPPCl ($(1-2) \times 10^{-5}$ mol dm^{-3}) occurred for pyrrole, thiophene, aniline, 2-mercaptobenzimidazole, and 2-phenylimidazole concentrations up to ~0.1 mol dm^{-3}. A very weak reaction with FeTPPCl was found for pyridine ligand. The remaining ligands, i.e., imidazole, 1-methylimidazole, 1-butylimidazole, 1-(diethoxymethyl)-imidazole, 2-methylimidazole, 3,5-diamino-1,2,4-triazole, (3-aminopropyl)imidazole, and cyclohexyloamine, were found to react with FeTPPCl as manifested by profound changes in the porphyrin spectrum. Changes were qualitatively identical for all ligands except 3,5-diamino-1,2,4-triazole and manifested by a growth of the absorption peak at 416 nm and a decrease of the peak at 378 nm, both belonging to the Soret band.[31] Changes in the Q band of the spectrum were also observed (Figure 1).

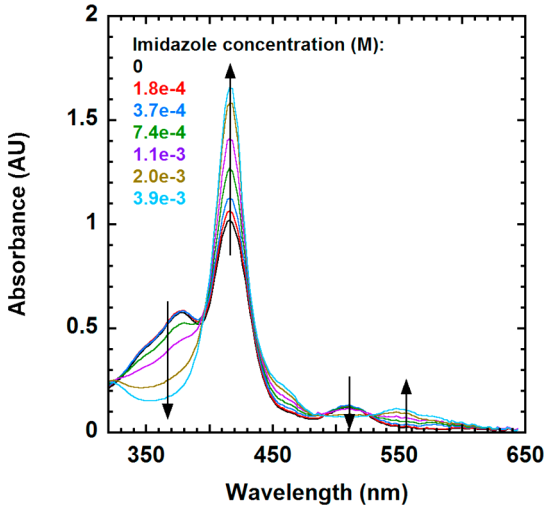

Figure 1. Spectra of ~1.07×10^{-5} mol dm^{-3} FeTPPCl in DCM upon addition of various quantities of imidazole. Optical path length 1 cm. Imidazole concentrations listed in the figure.

For all above ligands, well-defined isosbestic points indicated the presence of a single chemical equilibrium between the reaction substrates and products. At sufficiently high ligand to FeTPPCl concentration ratios, no measurable or very limited absorbance changes could be detected upon further ligand concentration increase. Spectra measured under such conditions were found to correspond to 1:2 rather than 1:1 complexes between FeTPPCl and the ligands. This conclusion was reached from a comparison of the results of nonlinear fitting of the observed absorbance changes when the reaction stoichiometry was assumed to be 1:1 or 1:2 or both 1:1 and 1:2. The fit quality obtained for 1:2 reaction stoichiometry was found incomparably better than that for 1:1 stoichiometry. The fit quality was very slightly improved when both 1:1 and 1:2 stoichiometries were taken into account, but the results indicated that the complexes with 1:1 stoichiometry had a rather negligible influence on the overall mass balance and the measured spectra, in accordance with the presence of isosbestic points in the spectra of the mixed FeTPPCl + ligand solutions (Figure 1). While the measured 1:2 stoichiometry seemed rather unexpected for the low concentrations of the reactants used in the present work, literature data confirm the correctness of the present conclusion.[32] Due to the low dielectric permittivity of DCM,[33] the reaction between the complexing agents and the porphyrin can be expressed as follows

$$\mathrm{FeTPPCl} + 2\mathrm{L} \rightleftharpoons \mathrm{FeTPPL}_2^{+} + \mathrm{Cl}^{-} \quad (1)$$

The equilibrium constants for reaction 1 were extracted from nonlinear fitting of the dependencies of absorbance ratios $A(\lambda 1 = 416\ \mathrm{nm})/A(\lambda 2 = 378\ \mathrm{nm})$ vs ligand concentration (Figure 2)

$$A_{\lambda 1}/A_{\lambda 2} = (\varepsilon_{\lambda 1}^{\mathrm{FeTPPCl}} + \varepsilon_{\lambda 1}^{\mathrm{FeTPPL2}}\beta_2 C_{\mathrm{L}}^{\ 2}) / (\varepsilon_{\lambda 2}^{\mathrm{FeTPPCl}} + \varepsilon_{\lambda 2}^{\mathrm{FeTPPL2}}\beta_2 C_{\mathrm{L}}^{\ 2}) \quad (2)$$

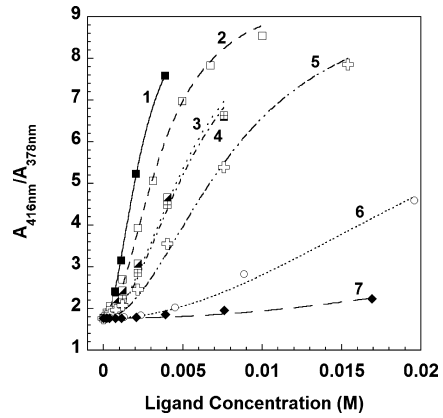

Figure 2. Ratios of absorbance at 416 nm to that at 378 nm measured for FeTPPCl solutions in DCM vs concentration of various ligands. Optical path length 1 cm. Ligands and FeTPPCl concentrations (mol dm^{-3}): (1) imidazole, $C_{\mathrm{FeTPPCl}} = 1.07 \times 10^{-5}$; (2) 1-(3-aminopropyl)-imidazole, $C_{\mathrm{FeTPPCl}} = 1.49 \times 10^{-5}$; (3) 1-butylimidazole, $C_{\mathrm{FeTPPCl}} = 1.61 \times 10^{-5}$; (4) 1-diethoxymethylimidazole, $C_{\mathrm{FeTPPCl}} = 1.73 \times 10^{-5}$; (5) 1-methylimidazole, $C_{\mathrm{FeTPPCl}} = 1.47 \times 10^{-5}$; (6) 2-methylimidazole, $C_{\mathrm{FeTPPCl}} = 1.35 \times 10^{-5}$; (7) cyclohexyloamine, $C_{\mathrm{FeTPPCl}} = 1.50 \times 10^{-5}$.

where $\varepsilon_{\lambda 1}$ and $\varepsilon_{\lambda 2}$ are the extinction coefficients at $\lambda 1 = 416$ nm and $\lambda 2 = 378$ nm (known for FeTPPCl), β_2 is the equilibrium constant, and C_{L} is the axial ligand concentration. The equilibrium constants β_2 are listed in Table 1. Examination of the data in Table 1 reveals that unsubstituted imidazole is the strongest axial ligand for FeTPPCl, followed by N-substituted imidazoles, 2-substituted imidazoles, and cyclohexyloamine. The much weaker complexation of FeTPPCl by 2-phenyl-imidazole compared to 2-methylimidazole and by aniline compared to cyclohexyloamine are most likely associated with unfavorable steric effects for the ligands containing big phenyl groups. The same effect is probably responsible for the virtual lack of FeTPPCl complexation by 2-mercaptobenzimidazole. As indicated by the lack of interaction between pyrrole and FeTPPCl, reactions between imidazoles and FeTPPCl must involve the unsubstituted aromatic nitrogen in the imidazole moiety. Semiempirical calculations using the PM3 model[34,35] demonstrated that imidazoles act as π-type ligands. In this light,

dx.doi.org/10.1021/jp5044249 | J. Phys. Chem. C 2014, 118, 19139−19149

Table 1. Cumulative Formation Constants for 1:2 Complexes of FeTPPCl with Various Ligands in DCM

ligand	β_2 (mol^{-2} dm^6)	$\log(\beta_2$ (mol^{-2} dm^6))
imidazole (Fe(III)TPPCl)	$(6.58 \pm 0.11) \times 10^5$	5.82
imidazole (Fe(II)TPP)[a]	$(3.67 \pm 0.72) \times 10^8$	8.56
1-(3-aminopropyl)imidazole	$(2.76 \pm 0.13) \times 10^5$	5.44
1-butylimidazole	$(1.19 \pm 0.11) \times 10^5$	5.08
1-diethoxymethylimidazole	$(1.10 \pm 0.05) \times 10^5$	5.04
1-methylimidazole	$(5.53 \pm 0.27) \times 10^4$	4.74
2-methylimidazole	$(5.45 \pm 0.24) \times 10^3$	3.74
cyclohexyloamine	$(8.33 \pm 0.74) \times 10^2$	2.92
pyridine	<100	<2
aniline	<100	<2
2-phenylimidazole	<100	<2
2-mercaptobenzimidazole	<100	<2

[a]Obtained from the reversible reduction potential of ~1 mM Fe(III)TPPCl in 0.1 mol dm^{-3} $TBAPF_6$ + ~0.1 mol dm^{-3} imidazole in DCM using cyclic voltammetry and assuming 2:1 complex stoichiometry.

the significantly weaker FeTPPCl complexation by pyridine, also a π-type ligand, is explained by a mismatch of the respective donor and acceptor orbital energies.

The complexing ability of 3,5-diamino-1,2,4-triazole, which is virtually insoluble in DCM, was compared to that of unsubstituted imidazole using a mixed 9:1 acetone/water mixture for ligand stock solutions and acetone solution of the porphyrin. The effects of imidazole on the FeTPPCl spectrum in the acetone/water mixture were almost identical with those observed in pure DCM solutions (see above). The triazole complexing ability was found to be weaker as demonstrated by around 1 order of magnitude higher triazole concentration required to cause noticeable changes in the porphyrin spectrum. Moreover, the two major components of the Soret band were found to shift with triazole (water?) concentration, there was virtually no increase of the longer wave component of the Soret band, and no isosbestic points were detected. Such changes are consistent with more complex reaction stoichiometry, e.g., stepwise and competitive complexation of the porphyrin by triazole and water. Similar effects would have been expected for the ligands weaker than imidazoles if mixed acetone + water solvents had been applied.

Data presented above indicate that imidazoles, due to their exceptionally strong bonding to $FeTPP^+$, are most promising candidates to act as internal electron donors and possibly facilitate oxygen reduction catalyzed by the porphyrin.

SPECTROELECTROCHEMISTRY

Spectroelectrochemical experiments were performed with deoxygenated and oxygenated DCM solutions of FeTPPCl in the absence and presence of excess imidazole. Two electrochemical techniques were used to measure the spectral changes associated with reduction processes of FeTPPCl, namely, chronoamperometry and cyclic voltammetry. Experiments were limited to the first reduction processes.

In the absence of oxygen, both uncomplexed and imidazole complexed FeTPPCl were reduced reversibly. Representative spectra measured during the transport-controlled reductions and corresponding voltammograms are presented in Figure 3. Full spectrum recovery was observed for both uncomplexed and complexed porphyrin upon reoxidation of their reduced forms (Figures S1 and S2, Supporting Information). Similar

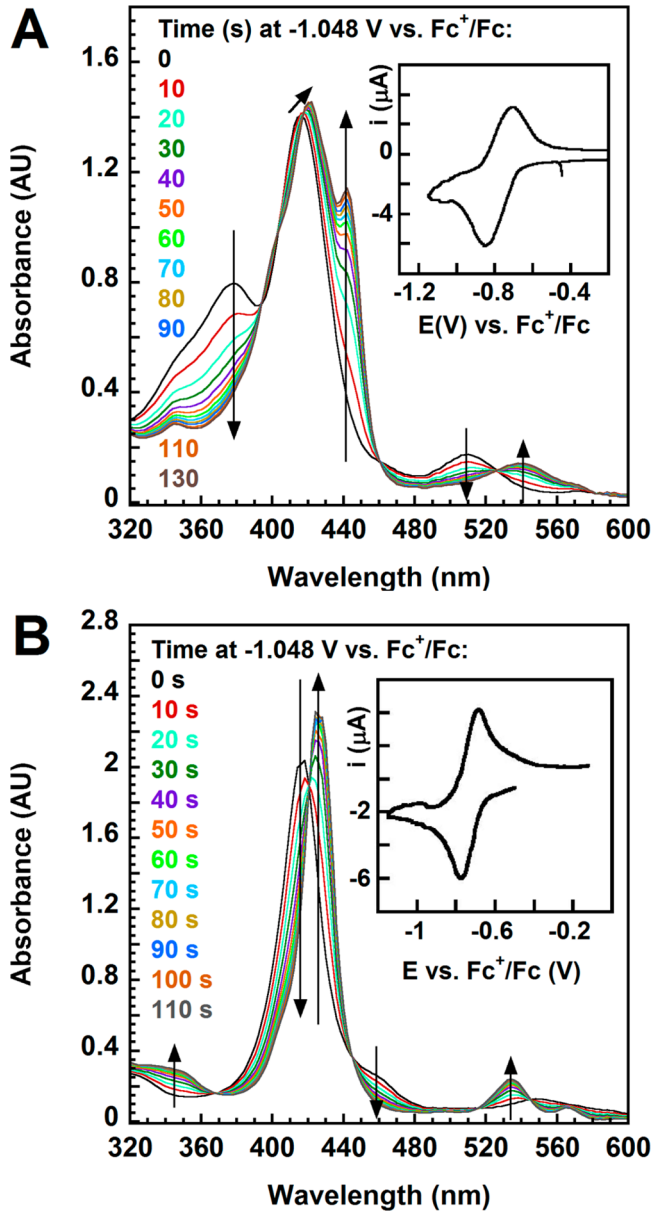

Figure 3. Spectroelectrochemistry for the first reduction processes of 2.78×10^{-4} mol dm^{-3} FeTPPCl (A) and 2.67×10^{-4} mol dm^{-3} FeTPPCl + 0.1 mol dm^{-3} imidazole (B) in deoxygenated 0.1 mol dm^{-3} $TBAPF_6$ in DCM under transport control conditions. Reduction potential −1.048 V vs ferrocene. Respective voltammograms recorded at a scan rate of 2 mV s^{-1} using the same experimental setup are shown in the insets.

reversible spectroelectrochemistry was observed when the reduction and reoxidation reactions were performed under cyclic voltammetric conditions (Figures S3 and S4, Supporting Information).

The voltammograms shown in the insets in Figure 3 exhibit characteristics largely determined by semiinfinite rather than thin layer diffusion in spite of the very low scan rate (2 mV s^{-1}) used. This behavior is easily explained by a comparatively thick (0.5 mm) solution layer undergoing reduction and oxidation and by the smaller geometric dimensions of the working Au electrode than those of the thin layer compartment.

In the presence of oxygen, the reduction processes of both complexed and uncomplexed porphyrin were electrochemically

dx.doi.org/10.1021/jp5044249 | J. Phys. Chem. C 2014, 118, 19139−19149

irreversible, as demonstrated by a significant separation between the reduction and the oxidation processes (Figure 4). The extent of chemical reversibility of the reduction

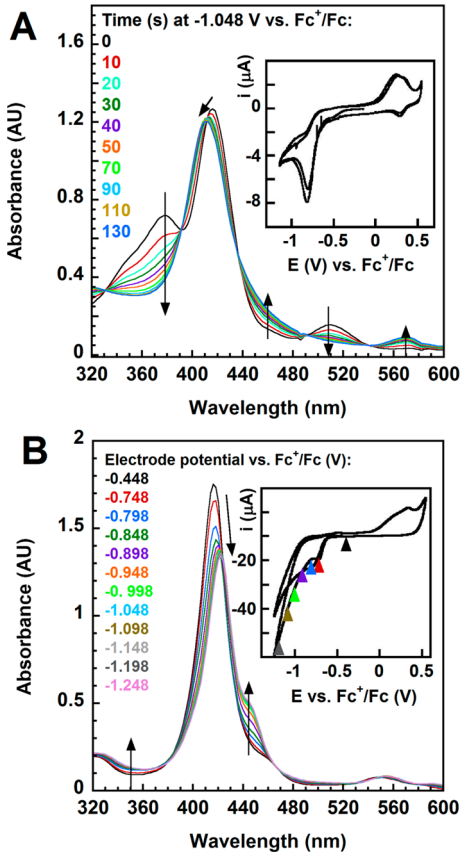

Figure 4. Spectroelectrochemistry for the first reduction processes of 2.58×10^{-4} mol dm^{-3} FeTPPCl (A) and 2.67×10^{-4} mol dm^{-3} FeTPPCl + 0.1 mol dm^{-3} imidazole (B) in oxygenated 0.1 mol dm^{-3} $TBAPF_6$ in DCM. Transport-controlled reaction for FeTPPCl solution (A) monitored at a constant potential of −1.048 V vs ferrocene (see the respective voltammogram recorded at a scan rate of 2 mV s^{-1} in the inset). Kinetically controlled reaction for FeTPPCl + imidazole solution (B) monitored under voltammetric conditions at a scan rate of 2 mV s^{-1}. Respective voltammogram with colored arrows matching the colors of the measured spectra is presented in the inset.

processes was assessed from the spectra measured upon reoxidation of the respective reduced solutions. No spectrum recovery was observed upon reoxidation of the reduced porphyrin in the presence of oxygen at +0.3 V vs ferrocene (Figure S5, Supporting Information). A partial spectrum recovery was observed upon reoxidation of the reduced porphyrin in its oxygenated solution containing imidazole (Figure S6, Supporting Information), but the origin of the recovery is unclear. Due to the lack of well-defined reduction/reoxidation peaks in the voltammograms of such solutions (Figure 4B, inset), spectroelectrochemical experiments were performed using exclusively cyclic voltammetry. Under such conditions, the time needed to scan the potential from the reduction to the respective oxidation reaction was around 600 s. During that time, some quantities of the complexed porphyrin and its reduction product(s) may have diffused, respectively, into and away from the thin layer compartment, which may explain the apparent spectrum recovery. Moreover, unidentified chemical compounds with spectra similar to the original porphyrin may have also been generated during the anodic scans.

While the mostly semiinfinite character of diffusion in the spectroelectrochemical cell precludes any rigorous quantitative data treatment, some important conlusions regarding the stoichiometry of the reactions can still be made based on the data collected. The peak current measured for oxygenated FeTPPCl solution is ∼30% higher than that measured in deoxygenated solution (Figures 3A and 4A). If the number of electrons transferred per FeTPPCl were the same, i.e., one in both cases, then the irreversible peak measured for the oxygenated solution should be lower due to the peak current dependence on the reaction transfer coefficient.[36] Consequently, the average number of electrons transferred in the oxygenated solution is higher than one. When the reduction is performed under diffusion-controlled potentiostatic conditions (chronoamperometry at −0.6 V vs AgQRE, −1.048 V vs Fc$^+$/Fc), the ratio of the reduction charges in oxygenated and deoxygenated porphyrin solutions (normalized for FeTPPCl concentration) is very close to 1 during the initial ∼10 s of the electrolysis but reaches 2 at longer reduction times (Figure 5).

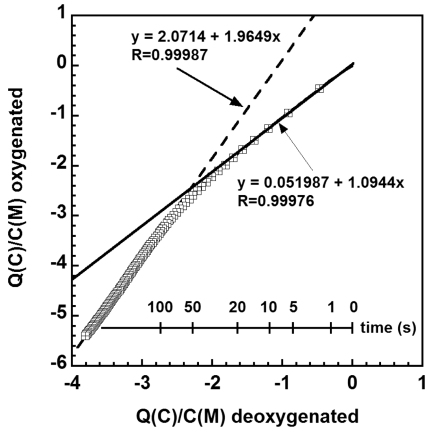

Figure 5. Relationship between the porphyrin concentration normalized charges of FeTPPCl reduction in the presence and absence of oxygen. Concentration of FeTPPCl 2.56×10^{-4} (oxygenated solution) and 2.78×10^{-4} mol dm^{-3} (deoxygenated solution). Only 5% of the measured points are shown in the graph.

This finding can be explained as follows. Since oxygen is reduced on Au at very high overpotentials,[37] the first step in the oxygenated solutions is one-electron reduction of the porphyrin (Fe(III)TPPCl) to Fe(II)TPP (Figure 3)

$$\mathrm{Fe(III)TPPCl} + \mathrm{e}^- \rightleftharpoons \mathrm{Fe(II)TPP} + \mathrm{Cl}^-(\mathrm{reversible}) \quad (3)$$

Fe(II)TPP is not a sufficiently strong reducing agent to reduce molecular O_2 to superoxide radical.[38] Instead, it forms a coordination compound ($[O_2\cdots\mathrm{Fe(II)TPP}]$) where at least partial charge transfer from the metal to oxygen takes place

$$\mathrm{Fe(II)TPP} + \mathrm{O}_2 \rightleftharpoons [\mathrm{O}_2{}^{\delta-}\cdots\mathrm{Fe(II} + \delta)\mathrm{TPP}](\mathrm{reversible}) \quad (4)$$

The above complex can be subsequently reduced by another electron to form $[(\mathrm{O}_2{}^{2-})\cdots\mathrm{Fe(III)TPP}]^-$[39]

$$[\mathrm{O}_2{}^{\delta-}\cdots\mathrm{Fe(II} + \delta)\mathrm{TPP}] + \mathrm{e}^- \rightarrow [(\mathrm{O}_2{}^{2-})\cdots\mathrm{Fe(III)TPP}]^- \quad (5)$$

The total number of electrons transferred in the above reaction sequence should be equal to 2 in the absence of any

dx.doi.org/10.1021/jp5044249 | J. Phys. Chem. C 2014, 118, 19139−19149

parasitic processes. However, if any of the partially reduced species, i.e., Fe(II)TPP or $O_2^{\delta-}\cdots$Fe(II+δ)TPP, were irreversibly lost during the reduction, the expected number of electrons should be less than one. Small quantities of the partially reduced compounds may diffuse away from the thin layer compartment and thus be essentially lost for further reduction (eq 5), but such a process could possibly explain only a slight negative departure of the number of electrons from 2. To the contrary, the initial number of electrons in the oxygenated solution is close to one, which implies that $O_2^{\delta-}\cdots$Fe(II+δ)TPP either reacted almost completely to an electrochemically inactive product or was not generated at all during the first few seconds of electrolysis. Spectra recorded during the reduction have well-defined isosbestic points (Figure 4), which suggests that only two porphyrin species contributed to the measured absorption. The reduced species contributing to the spectra cannot be Fe(II)TPP, because its spectrum (Figure 3A) is completely different than that evolving during electrolysis of the oxygenated solution (Figure 4A). Consequently, the only plausible explanation of the single electron transferred in the initial stages of the electrolysis is a parasitic homogeneous reaction of [$O_2^{\delta-}\cdots$Fe(II+δ)TPP], whose products do not contribute significantly to both the spectra and the electrochemical reaction. The presence of such a side reaction seems to be confirmed by the voltammogram of the oxygenated solution, which exhibits a lower reoxidation charge than the reduction charge (Figure 4A) and already mentioned somewhat incomplete reversibility of the spectra upon reoxidation. Apparently, the spectra of the products of the side reaction are sufficiently similar to that of [(O_2^{2-})$\cdots$Fe(III)TPP]$^-$, so that they do not seriously distort the isosbestic points. The postulated side reaction must involve impurities present in the solvent or the electrolyte, as suggested by the gradual transition from the one-electron to the two-electron reaction. After sufficiently long reduction times, the impurities are exhausted and [$O_2^{\delta-}\cdots$Fe(II+δ)TPP] can exclusively undergo the second electron transfer, which produces [(O_2^{2-})$\cdots$Fe(III)TPP]$^-$ or perhaps its protonated form [(HO_2^-)$\cdots$Fe(III)TPP], which may be formed through reaction of O_2^{2-} with traces of water likely present in solution. The above explanations of the spectroelectrochemistry remain in agreement with the fact that oxygen concentration in oxygen-saturated dichloromethane solutions exceeds that of the porphyrin by almost 35 times[40] and that none of the reduced oxygen species itself absorbs light below 300 nm.[41]

The spectrum of the doubly reduced species (Figure 4A) identified as [(O_2^{2-})$\cdots$Fe(III)TPP]$^-$ or [(HO_2^-)$\cdots$Fe(III)TPP] is very similar to the spectrum of FeTPPCl axially coordinated by imidazoles (Figures 1 and 4) . The finding agrees with the fact that the iron center in both imidazole-coordinated porphyrin and [(O_2^{2-})$\cdots$Fe(III)TPP]$^-$ remains in the +3 oxidation state. In order to confirm that the spectrum measured for the reduced oxygenated solution of FeTPPCl indeed corresponds to the porphyrin coordinated by peroxide (or hydroperoxide) anion, an experiment was performed where a DCM solution of FeTPPCl was brought in contact with an aqueous Na_2O_2 solution prepared by mixing a concentrated NaOH solution with 30% H_2O_2. After a few minutes of shaking the reaction mixture and allowing it to spontaneously separate into distinct aqueous and organic phases, a spectrum of the DCM solution was measured. As expected, the spectrum (Figure 6) was very similar to that obtained for the reduced oxygenated solution of FeTPPCl. After similar reaction

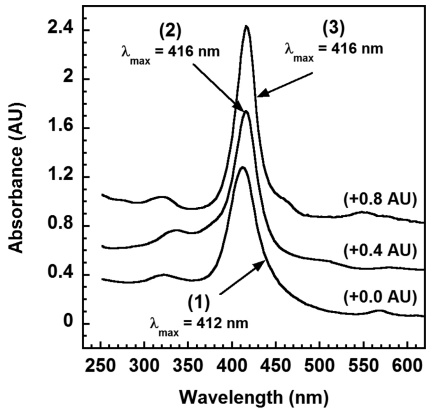

Figure 6. Spectra of axially coordinated iron tetraphenylporphyrins generated under various conditions: (1) 2.58×10^{-4} mol dm^{-3} Fe(III)TPPCl after an exhaustive electrolysis in oxygen-saturated 0.1 mol dm^{-3} solution of $TBAPF_6$ in DCM, (2) 1.23×10^{-5} mol dm^{-3} Fe(III)TPPCl after reaction with concentrated aqueous Na_2O_2 solution (see text), and (3) 1.07×10^{-5} mol dm^{-3} Fe(III)TPPCl + 7.6×10^{-3} mol dm^{-3} imidazole in DCM.

between FeTPPCl and neutral 30% H_2O_2, only a very small decrease of the absorbance of the organic phase was observed without any changes of the shape of the spectrum. Consequently, the interaction between peroxide (O_2^{2-}) or hydroperoxide (HO_2^-) anion and the metal center is too weak to promote dissociation of H_2O_2 and formation of the respective O_2^{2-}/HO_2^- complex with Fe(III)TPP$^+$. This also suggests that iron tetraphenylporphyrin will not catalyze H_2O_2 reduction in acidic media.

Reduction of oxygen catalyzed by imidazole-coordinated FeTPPCl in DCM solutions involves a higher number of electrons than that transferred in ORR catalyzed by FeTPPCl, as indicated by significantly higher reduction currents measured for the oxygenated FeTPPCl + imidazole solutions compared to those recorded for the oxygenated FeTPPCl solutions (Figure 4A and 4B). As previously mentioned, the associated spectral changes were not fully reversible upon reoxidation of the solution. We also performed spectrophotometric experiments, where FeTPPCl + imidazole solutions in DCM were brought in contact with aqueous H_2O_2 (30%) and Na_2O_2 solutions. As opposed to the FeTPPCl solutions without imidazole (vide supra), complete degradation of the porphyrin manifested by a full discoloration of the organic phase was observed when H_2O_2 was used. Irreversible changes were also observed for Na_2O_2. In that case, however, the maximum absorbance of the organic phase dropped around 4 times and remained stable after that. It is possible that in the alkaline medium, μ-oxo dimer of the porphyrin was formed as a result of the reaction involving Fe(III)TPP(imidazole)$_2$ and hydroxyl anions.[42]

The results presented in this section suggest that axial complexation of iron in the porphyrin and possibly in its other macrocyclic complexes by imidazoles can enhance the catalytic activity of the macrocycles for ORR in aqueous media. However, as demonstrated by the irreversible degradation of FeTPPCl + imidazole solutions in the presence of H_2O_2, axial complexation of such macrocycles may also lead to a decreased durability of the active site if hydrogen peroxide is either the final or the transitional product of the ORR.

dx.doi.org/10.1021/jp5044249 | J. Phys. Chem. C 2014, 118, 19139−19149

AXIAL COMPLEXATION OF FETPPCL BY POLYVINYLIMIDAZOLE

Spectrophotometry of FeTPPCl + PVI solutions in 1:1 methanol + acetone mixtures (Figure 7) shows that FeTPPCl

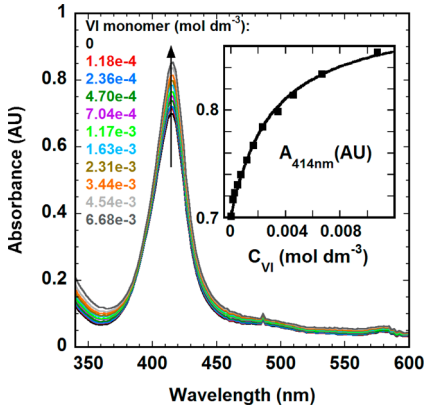

Figure 7. Equilibrium between 1.55×10^{-5} mol dm^{-3} Fe(III)TPPCl and polyvinylimidazole in 1:1 (v/v) CH_3OH + $(CH_3)_2CO$ measured by spectrophotometry. Imidazole concentrations listed in the figure. (Inset) Absorbance at λ_{max} (416 nm) plotted vs the monomer concentration.

spectrum in CH_3OH + $(CH_3)_2CO$ is different than that in much less polar dichloromethane (Figure 1). This is most likely due to dissociation of chloride anion in the polar solvent and solvation of the iron center. The changes in FeTPPCl spectra upon addition of PVI are similar to those produced by monomeric imidazoles, i.e., they result in an increase of the Soret band (Figure 7) and can be linked to axial complexation of FeTPP by PVI. It is also worth mentioning that a very slight increase of the measured absorbance with PVI concentration was observed in the entire wavelength range (Figure 7). That increase originates from light scattering by the polymer. Therefore, the spectra presented in Figure 7 are limited to lower PVI concentrations, where the said effect had only a minor influence on the measured absorbance.

In order to quantify the porphyrin interactions with PVI, various theoretical models were used to fit the observed spectral changes. Beyond simple models, e.g., assuming individual PVI molecules to be capable to react exclusively with a single porphyrin molecule, more complex approaches were also used. In some models, polyvinylimidazole molecules were treated as "surfaces" with a limited number of sites that can interact with FeTPPCl. Those interactions were described by known adsorption isotherms, such as Langmuir[43] or Temkin,[44] where the repulsive interactions between individual porphyrin molecules were, respectively, either neglected or taken into account. Somewhat unexpectedly, the best overall fit, shown in Figure 7 for 414 nm (λ_{max} for the uncomplexed porphyrin), was obtained for the simplest model, where imidazole monomers in PVI were treated as independent ligands interacting with single porphyrin molecules and the stoichiometry of the reaction was 1:1. The equilibrium constant β_1 obtained from the fit equals $(3.26 \pm 0.30) \times 10^2$ mol^{-1} dm^3, and the extinction coefficient of the complex at 414 nm is $(7.43 \pm 0.06) \times 10^4$. λ_{max} for the Soret band of the complex could not be determined, but it is $\geq$416 nm, and the extinction coefficient of the band is higher than 7.47×10^4 (Figure 7). Regardless of the apparent success of the simple model, the above numbers have to be treated with caution. This is because the assumption that the monomers in PVI molecules can be regarded as independent entities indirectly neglects the entropy differences between the PVI and its monomers and thus implies that the only driving force for the reaction is the enthalpy. In addition, light scattering by PVI molecules (vide supra) likely leads to an overestimated equilibrium constant for the complexation reaction. In spite of such uncertainties, the results demonstrate that immobilized imidazole groups, such as those in PVI, can be used as anchoring centers for FeTPPCl on a solid support.

OXYGEN REDUCTION CATALYSIS

Most imidazoles are readily soluble in water. In order to attach imidazole ligands to suitable catalyst supports and prevent their escape from the catalyst layer, two alternative approaches were used. In the first approach, reduced graphene oxide modified with 3-aminopropyl imidazole groups was applied as the support for the porphyrin. In the second approach, polyvinyl imidazole (PVI) was used as a component of the catalyst ink containing high surface area carbon (Vulcan XC72) and FeTPPCl. Five catalyst inks were prepared using comparable quantities of FeTPPCl. The first ink, herein denoted as #1, contained exclusively FeTPPCl and high surface area carbonaceous support (Vulcan XC72). The second ink (#2), in addition to FeTPPCl and Vulcan XC72 support, contained polyvinylimidazole. In the third ink (#3), 3-aminopropylimidazole-modified reduced graphene oxide (G-IMD) was used as a support for FeTPPCl. Finally, in two inks reduced ghraphene oxides modified with aliphatic amine groups, i.e., piperazine (RGO-NH, #4) and 2,2′-(ethylenedioxy)bis(ethylamine) (RGO-NH2, #5), were used as the catalyst supports. The composition of those inks and methods of PVI as well as G-IMD synthesis can be found in the Experimental Section. In addition, five inks containing only the catalyst supports, i.e., Vulcan, Vulcan + PVI, G-IMD, RGO-NH, and RGO-NH2, were also prepared.

The rotating ring disk electrode (RRDE) technique was used to characterize electrocatalytic activity and selectivity for oxygen reduction of the catalysts in 0.5 mol dm^{-3} H_2SO_4 solutions. Since the activities of all studied catalysts were found to change with time, multiple voltammetric cycles between 1 and 0 V vs the reference (Pt, 6% H_2 in Ar, 0.5 mol dm^{-3} H_2SO_4) were recorded. With the exception of ink #2 (Vulcan XC72 + PVI + FeTPPCl), whose activity slightly increased from the first to the second cycle, all catalysts exhibited maximum ORR activity in the initial cycle. The respective voltammograms are shown in Figure 8. Some of the voltammograms in Figure 8 exhibit a hysteresis, which reflects instability (restructuring) of the as-prepared catalyst layers and the resulting inadequate background corrections. Such effects were strongest for graphenes modified with aliphatic amine groups. Since the overall catalytic activities of these materials with and without FeTPPCl were rather low, no further study of these effects was performed. The activities of the porphyrin on the reduced graphene oxides modified with aliphatic amine groups (RGO-NH and RGO-NH2) are comparable, and the reduction occurs predominantly via a two-electron route. Interestingly, the activity of RGO-NH2 alone has been found higher than that of RGO-NH2 + FeTPPCl. Also, no evident difference in catalytic activity has been detected between RGO-NH and RGO-NH + FeTPPCl (Figure 8). While no detailed study of those effects has been performed, it seems possible that the $\pi-\pi$ stacking interactions between the modified graphene particles are enhanced in the

dx.doi.org/10.1021/jp5044249 | J. Phys. Chem. C 2014, 118, 19139−19149

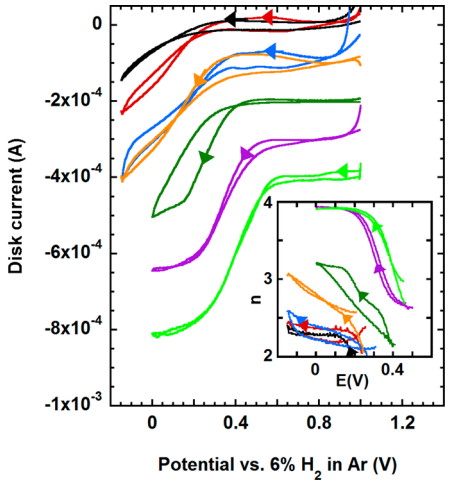

Figure 8. Background-corrected RRDE voltammograms of oxygen-saturated 0.5 mol dm^{-3} H_2SO_4 solutions recorded for various ORR catalysts. Rotation rate 400 rpm. Scan rate 10 mV s^{-1}. (Inset) Number of electrons (n) transferred in ORR determined from the measured ring current at 1.2 V.[45] The value of n is 2 when H_2O_2 is the exclusive product of ORR, n is 3, when 50% of oxygen is reduced to water and 50% to hydrogen peroxide, and n = 4 when oxygen is reduced completely to water. Catalysts: RGONH2, red; RGONH2 + Fe(III)TPPCl, black; RGONH, blue; RGONH + Fe(III)TPPCl, orange; Vulcan + Fe(III)TPPCl, dark green; G-IMD + Fe(III)TPPCl, purple; Vulcan + PVI + Fe(III)TPPCl, light green.

presence of the porphyrin. Such an effect may lead to a decrease in the number of exposed iron active sites as well as a drop in the accessible surface area of the modified graphenes. As the latter exhibit catalytic activity in ORR comparable to that of the porphyrin, the net result may be paradoxically an overall drop in activity (RGO-NH2 + FeTPPCl vs RGO-NH2) or no activity change (RGO-NH + FeTPPCl vs RGO-NH). On the other hand, oxygen reduction catalysis is significantly enhanced when Vulcan + PVI and G-IMD are used as catalyst supports. The half-wave potentials for ORR are shifted anodically in excess of 200 mV. In addition, the number of electrons involved in ORR increases with the cathodic overpotential from 2 (hydrogen peroxide) to 4 (water). While the half-wave potential change results in part from the shift of the reversible Fe(III)/Fe(II) potential resulting from the stronger coordination of the reduced state by the imidazole moieties (vide supra), without any doubt it is also caused by an acceleration of the intrinsic kinetics of the ORR. The enhancement of ORR catalysis in the presence of PVI and G-IMD results from the axial complexation of FeTPPCl by imidazole groups present in the catalyst supports. The conclusion is supported by the spectrophotometry of FeTPPCl solutions in the presence of imidazoles and by the spectroelectrochemical data for deoxygenated/oxygenated FeTPPCl and FeTPPCl + imidazole solutions. The lack of a similar enhancement for RGO-NH and RGO-NH2 supports corroborates with the substantially weaker complexation of the porphyrin by aliphatic nitrogen (vide supra). It is interesting to note that for both Vulcan + PVI and G-IMD catalyst supports there are effective paths for electron transfer from the support to the coordinated porphyrin even though both coordinating agents must separate the conductive phase from the porphyrin. Apparently, electronic $\pi-\pi$ interactions between the porphyrin and the graphitic rings of Vulcan and G-IMD are still present and facilitate electron tunneling from the support to the porphyrin and eventually to its active center.

Axial complexation of iron in the porphyrin is an effective means of enhancing the catalytic activity of the macrocycle, but it is not as effective as a method to permanently anchor the porphyrin to the support. The durability of all catalysts in acidic media was not satisfactory. In all cases, the activity of the catalyst was found to decrease from cycle to cycle during the RRDE experiments. The representative plots are shown in Figure 9.

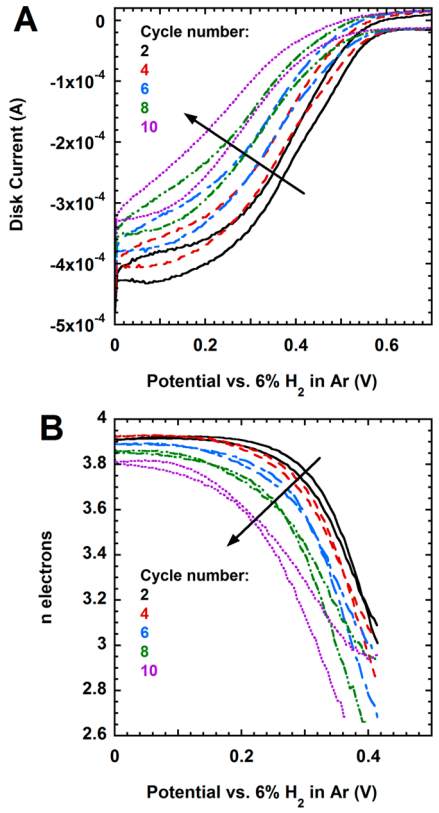

Figure 9. Dependencies of (A) oxygen reduction currents and (B) number of electrons transferred on Vulcan + PVI + Fe(III)TPPCl catalyst in oxygen-saturated 0.5 mol dm^{-3} H_2SO_4 solution on the cycle number under RRDE conditions. Rotation rate 400 rpm. Scan rate 10 mV s^{-1}.

The gradual decrease of the catalytic activity, accompanied by a decrease in the catalyst selectivity for water, is most likely caused by protonation of the aromatic nitrogen in imidazole moiety that makes the complexation reaction less favorable. It has to be noted that oxygen reduction catalysis is possible only when at least one axial position of the iron center is accessible to oxygen, i.e., it is not occupied by a strong ligand. In the present case, the porphyrin is held in place through the inherently weaker single axial coordination (vide supra). While the strength of the imidazole−Fe bond may be temporarily enhanced during ORR by a reduced oxygen species (e.g., O_2^{2-}), which occupies the opposite axial site, only a weaker coordinated water remains in that site after reduction. Finally, as demonstrated in one of the previous sections, the porphyrin coordinated by imidazole is readily oxidized in the presence of 30% H_2O_2, and it seems possible that even significantly lower concentrations of peroxide generated during the ORR may contribute to the gradual loss of the catalyst activity (Figure 9).

dx.doi.org/10.1021/jp5044249 | J. Phys. Chem. C 2014, 118, 19139−19149

Due to the durability issues described above, background correction of the measured currents was problematic. The background-corrected ORR currents were different in the forward and reverse scans (Figures 8 and 9). In order to extract the best possible kinetic data, averages of the forward and reverse currents were used in kinetic analysis.

Figure 10 shows Tafel plots obtained for the two most active catalysts. As seen in Figure 10, the catalyst utilizing PVI as a

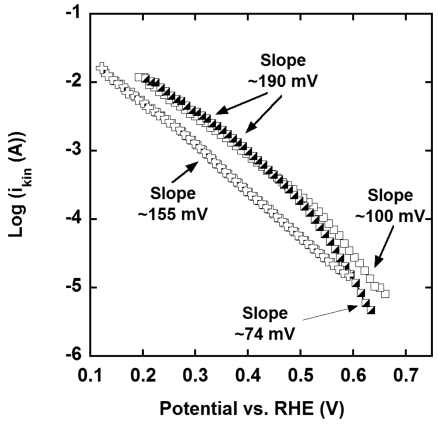

Figure 10. Tafel plots for ORR in 0.5 mol dm^{-3} H_2SO_4 on FeTPP(III)Cl + PVI + Vulcan XC72 (first scan, half-filled diamonds; second scan, open diamonds, see text) and FeTPP(III)Cl + G-IMD catalysts (crosses).

complexing/anchoring agent exhibits approximately three times higher initial activity at high overpotentials than the catalyst utilizing RGO functionalized with 3-aminopropylimidazole (G-IMD) as the support. This is because the complexation reaction by rather flexible PVI molecules with a high density of imidazole moieties is significantly more effective compared to 3-aminopropylimidazole ligands occupying fixed positions on the surface of G-IMD. Moreover, the $\pi-\pi$ stacking interactions such as those postulated above for RGO-NH and RGO-NH2 may have also contributed to the overall lower activity of the G-IMD + FeTPPCl compared to that of the Vulcan + PVI + FeTPPCl.

The Tafel plots shown in Figure 10 have relatively high slopes, similar to those observed for many pyrolyzed Fe/N/C catalysts at high overpotentials.[6,46] However, there are also distinct differences between the imidazole ligated iron tetraphenyl porphyrins and the pyrolyzed Fe/N/C catalysts. These differences will be discussed in the next section.

DISCUSSION

The results presented in this paper demonstrate that axial coordination of iron in tetraphenylporphyrin environment enhances the catalytic activity of the porphyrin in ORR and improves the selectivity of the reaction for water. A similar effect of functional groups presumably present on the surface of the edge plane pyrolytic graphite (EPG) electrodes on ORR catalyzed by two iron porphyrins was postulated more than 20 years ago by Shi and Anson[14] and more recently also demonstrated by Elbaz and co-workers for Co porphyrins.[47−49] We hypothesize that the effect observed by us is a consequence of not only an increase of the electron density on the axially coordinated iron center but also the specific complex geometry. Indeed, as demonstrated herein and in previous work,[32] coordination of two axial sites of iron porphyrins is preferred over single axial site coordination. Even though the catalytic activity of imidazole-coordinated iron tetraphenylporphyrin is superior to that of the uncomplexed porphyrin, it is lower than that of state-of-the-art pyrolyzed Fe/N/C catalysts.[2,3] The latter frequently promote "direct" four-electron ORR and are unable to reduce molecular H_2O_2,[6,46] whereas uncomplexed iron tetraphenylporphyrin promotes H_2O_2 formation. These differences are in conflict with seemingly similar coordination environments of iron in Fe(II)TPP and that postulated[7,8] for heat-treated Fe/N/C catalysts. In both cases, Fe is coordinated by an aromatic ligand providing an N_4 (or N_{2+2}) square planar environment, i.e., porphyrin ring in FeTPPCl and pyridinic rings embedded in graphene plane(s) in Fe/N/C catalysts.

The axial ligation of the iron tetraphenylporphyrin by imidazoles improves the selectivity of ORR for water and thus makes the reaction stoichiometry similar to that observed for state-of-the-art Fe/N/C catalysts. However, to the authors' knowledge, there are no reports indicating the presence of a subsurface axial coordination of the metal centers in heat-treated catalysts. Moreover, the Tafel plots for ORR on numerous Fe/N/C catalysts exhibit a significant curvature,[6] whereas the Tafel plots for the axially coordinated iron tetraphenylporphyrin are essentially linear (Figure 10). Such differences indicate the presence of yet undefined factors that determine the ORR catalysis by the seemingly similar $Fe-N_4$ centers in porphyrins and heat-treated catalysts in spite of the similar ORR mechanisms proposed for both classes of catalysts.[6,46] One of such factors may be a unique electronic environment of the active sites in heat-treated Fe/N/C catalysts created by a highly delocalized cloud of π electrons on their surface. On the other hand, the results presented in this paper demonstrate that the geometry of coordination plays a substantial role in the strength of interaction between the axial ligand(s) and the metal center. Coordination of both axial positions in FeTPP, which results in nearly octahedral complex geometry, is energetically much more favorable than single axial site coordination, which results in approximately square pyramidal geometry of the complex. Consequently, it is unclear, whether the differences between the activities and the selectivities of the axially coordinated iron tetraphenylporphyrin and those of state of the art Fe/N/C catalysts reflect predominantly differences in the strength of the "push effect" or also differences in its geometry (trans effect[50]). The question becomes even more puzzling in the light of a recent paper, where it is postulated that iron nanoparticles may play a role in ORR on Fe/N/C catalysts.[8] In spite of such uncertainties, the data presented in this paper show the great potential that lies in a controlled alteration of the electronic and other properties of metals coordinated by macrocyclic ligands as a means to create catalysts tailored to specific applications. While the present study has not resulted in crafting an ORR catalyst that outperforms state-of-the-art ones, it gives clues as to what steps need to be taken to make a better catalyst. For instance, by permanently attaching an axial ligand to iron porphyrin and creating a hydrophobic environment around it one could mitigate the durability problem related to ligand protonation.

ASSOCIATED CONTENT

Supporting Information

The Supporting Information contains spectroelectrochemical data obtained for (i) the reoxidation of deoxygenated and oxygenated FeTPPCl solutions and deoxygenated FeTPPCl + imidazole solutions under potentiostatic conditions, (ii) the

dx.doi.org/10.1021/jp5044249 | J. Phys. Chem. C 2014, 118, 19139−19149

reduction of deoxygenated FeTPPCl and FeTPPCl + imidazole solutions under voltammetric conditions (scan rate 2 mV/s), and (iii) the reoxidation of oxygenated FeTPPCl + imidazole solutions under voltammetric conditions (scan rate 2 mV/s). Figures S1−S6. This material is available free of charge via the Internet at http://pubs.acs.org.

AUTHOR INFORMATION

Corresponding Author

*E-mail: jerzy@lanl.gov, j.chlistunoff@gmail.com.

Author Contributions

The manuscript was written through contributions of all authors. All authors have given approval to the final version of the manuscript.

Notes

The authors declare no competing financial interest.

ACKNOWLEDGMENTS

Financial support from the University of California (grant 12-LR-237440) is gratefully acknowledged.

ABBREVIATIONS

AIBN, 2,2′-azobis(isobutyronitrile); DCM, dichloromethane; G-IMD, reduced graphene oxide with covalently linked 3-aminopropylimidazole; ORR, oxygen reduction reaction; PVI, polyvinylimidazole; PEFC, polymer electrolyte fuel cell; RGO, reduced graphene oxide; RGO-NH, reduced graphene oxide with covalently linked piperazine; RGO-NH2, reduced graphene oxide with covalently linked 2,2′-(ethylenedioxy)bis-(ethylamine); RHE, reversible hydrogen electrode; RRDE, rotating ring disk electrode

REFERENCES

(1) https://www1.eere.energy.gov/hydrogenandfuelcells/accomplishments.html.

(2) Proietti, E.; Jaouen, F.; Lefèvre, M.; Larouche, N.; Tian, J.; Herranz, J.; Dodelet, J.-P. Iron-based Cathode Catalyst with Enhanced Power Density in Polymer Electrolyte Membrane Fuel Cells. *Nat. Commun.* **2011**, *2*, 416−424.

(3) Wu, G.; More, K. L.; Johnston, C. M.; Zelenay, P. High-Performance Electrocatalysts for Oxygen Reduction Derived from Polyaniline, Iron, and Cobalt. *Science* **2011**, *332*, 443−447.

(4) Jaouen, F.; Lefèvre, M.; Dodelet, J.-P.; Cai, M. Heat-treated Fe/N/C Catalysts for O_2 Electroreduction: Are Active Sites Hosted in Micropores? *J. Phys. Chem. B* **2006**, *110*, 5553−5558.

(5) Jaouen, F.; Charreteur, F.; Dodelet, J.-P. Fe-based Catalysts for Oxygen Reduction in PEMFCs - Importance of the Disordered Phase of the Carbon Support. *J. Electrochem. Soc.* **2006**, *153*, A689−A698.

(6) Chlistunoff, J. RRDE and Voltammetric Study of ORR on Pyrolyzed Fe/Polyaniline Catalyst. On the Origins of Variable Tafel Slopes. *J. Phys. Chem. C* **2011**, *115*, 6496−6507.

(7) Lefèvre, M.; Dodelet, J.-P.; Bertrand, P. Molecular Oxygen Reduction in PEM Fuel Cells: Evidence for the Simultaneous Presence of Two Active Sites in Fe-based Catalysts. *J. Phys. Chem. B* **2002**, *106*, 8705−8713.

(8) Tylus, U.; Jia, Q.; Strickland, K.; Ramaswamy, N.; Serov, A.; Atanassov, P. B.; Mukerjee, S. Elucidating Oxygen Reduction Active Sites in Pyrolyzed Metal−Nitrogen Coordinated Non-Precious-Metal Electrocatalyst Systems. *J. Phys. Chem. C* **2014**, *118*, 8999−9008.

(9) Pita, M.; Gutierrez-Sanchez, C.; Olea, D.; Velez, M.; Garcia-Diego, C.; Shleev, S.; Fernandez, V. M.; De Lacey, A. L. High Redox Potential Cathode Based on Laccase Covalently Attached to Gold Electrode. *J. Phys. Chem. C* **2011**, *115*, 13420−13428.

(10) Jasinski, R. New Fuel Cell Cathode Catalyst. *Nature* **1964**, *201*, 1212−1213.

(11) Jasinski, R. Cobalt Phthalocyanine as a Fuel Cell Cathode. *J. Electrochem. Soc.* **1965**, *112*, 526−528.

(12) van Veen, J. A. R.; van Baar, J. F.; Kroese, C. J.; Coolegem, J. G. F.; de Wit, N.; Colijn, H. A. Oxygen Reduction on Transition-metal Porphyrins in Acid Electrolyte. 1. Activity. *Ber. Bunsen Ges. Phys. Chem.* **1981**, *85*, 693−700.

(13) Collman, J. P.; Denisevich, P.; Konai, Y.; Marrocco, M.; Koval, C.; Anson, F. C. Electrode Catalysis of the Four-Electron Reduction of Oxygen to Water by Dicobalt Face-to-Face Porphyrins. *J. Am. Chem. Soc.* **1980**, *102*, 6027−6036.

(14) Shi, C.; Anson, F. C. Catalytic Pathways for the Reduction of O_2 by Iron Tetrakis(4-N-methylpyridyl)porphyrin or Iron Tetraphenylporphyrin adsorbed on Edge Plane Pyrolytic Graphite Electrode. *Inorg. Chem.* **1990**, *29*, 4298−4305.

(15) Gano, K. W.; Myles, D. C. Progress toward the Synthesis of a Biomimetic Membrane. *Tetrahedron Lett.* **2000**, *41*, 4247−4250.

(16) Franzen, S.; Roach, M. P.; Chen, Y.-P.; Dyer, R. B.; Woodruff, W. H.; Dawson, J. H. The Unusual Reactivities of Amphirite Ornata Dehaloperoxidase and Notomastus Lobatus Chloroperoxidase do not Arise from a Histidine Imidazolate Proximal Heme Iron Ligand. *J. Am. Chem. Soc.* **1998**, *120*, 4658−4661.

(17) Dawson, J. H. Probing Structure-function Relations in Heme-containing Oxygenases and Peroxidases. *Science* **1988**, *240*, 433−439.

(18) Poulos, T. L. The Role of the Proximal Ligand in Heme Enzymes. *J. Biol. Inorg. Chem.* **1996**, *1*, 356−359.

(19) Goodin, D. B. When an Amide is More Like Histidine Than Imidazole: The Role of Axial Ligands in Heme Catalysis. *J. Biol. Inorg. Chem.* **1996**, *1*, 360−363.

(20) Rietjens, I. M. C. M.; Osman, A. M.; Veeger, C.; Zakharieva, O.; Antony, J.; Grodzicki, M.; Trautwein, A. X. On the Role of the Axial Ligand in Heme-based Catalysis of the Peroxidase and P450 Type Oxygen-transfer Reaction Mechanism. *J. Biol. Inorg. Chem.* **1996**, *1*, 372−376.

(21) Nam, W.; Han, H. J.; Oh, S.-Y.; Lee, Y. J.; Choi, M.-H.; Han, S.-Y.; Kim, C.; Woo, S. K.; Shin, W. New Insights into the Mechanisms of O−O Bond Cleavage of Hydrogen Peroxide and tert-Alkyl Hydroperoxides by Iron(III) Porphyrin Complexes. *J. Am. Chem. Soc.* **2000**, *122*, 8677−8684.

(22) McGuire, R., Jr.; Dogutan, D. K.; Teets, T. S.; Suntivich, J.; Shao-Horn, Y.; Nocera, D. G. Oxygen Reduction Reactivity of Cobalt(II) Hangman Porphyrins. *Chem. Sci.* **2010**, *1*, 411−414.

(23) Matson, B. D.; Carver, C. T.; Ruden, A. V.; Yang, J. Y.; Raugei, S.; Mayer, J. M. Distant Protonated Pyridine Groups in Water-soluble Iron Porphyrin Electrocatalysts Promote Selective Oxygen Reduction to Water. *Chem. Commun.* **2012**, *48*, 11100−11102.

(24) Tsuda, M.; Kasai, H. Imidazole Ligand Effect on O_2 Interaction with Metalloporphyrins. *Surf. Sci.* **2007**, *601*, 5200−5206.

(25) Zeng, Z. Y.; Gupta, S. L.; Huang, H.; Yeager, E. B. Oxygen Reduction on Poly(4-vinylpyridine)-Modified Ordinary Pyrolytic Graphite Electrodes with Adsorbed Cobalt Tetra-sulphonated Phthalocyanine in Acid Solutions. *J. Appl. Electrochem.* **1991**, *21*, 973−981.

(26) Cao, R.; Thapa, R.; Kim, H.; Xu, X.; Kim, M. G.; Li, Q.; Park, N.; Liu, M.; Cho, J. Promotion of Oxygen Reduction by a Bio-inspired Tethered Iron Phthalocyanine Carbon Nanotube-based Catalyst. *Nat. Commun.* **2013**, *4*, 2076−2082.

(27) Savin, G.; Burchard, W.; Luca, C.; Beldie, G. Global Solution Properties of Poly(N-vinylimidazole) in Ethanol. Macromolecules and Aggregates. *Macromolecules* **2004**, *37*, 6565−6575.

(28) Ohara, T. J.; Rajagopalan, R.; Heller, A. Glucose Electrodes Based on Cross-Linked $[Os(bpy)_2]^{+/2+}$ Complexed Poly(1-vinylimidazole) Films. *Anal. Chem.* **1993**, *65*, 3512−3517.

(29) Liu, W.; Koh, K. L.; Lu, J.; Yang, L.; Phua, S.; Kong, J.; Chen, Z.; Lu, X. Simultaneous Catalyzing and Reinforcing Effects of Imidazole-functionalized Graphene in Anhydride-cured Epoxies. *J. Mater. Chem.* **2012**, *22*, 18395−18402.

(30) Suwatchara, D.; Henstridge, M. C.; Rees, N. V.; Laborda, E.; Compton, R. G. Comparative Evaluation of the Symmetric and Asymmetric Marcus-Hush Formalisms of Electrode Kinetics - The

One-electron Oxidation of Tetraphenylethylene in Dichloromethane on Platinum Microdisk Electrodes. *J. Electroanal. Chem.* **2012**, *677*−*780*, 120−126.
(31) Shkirman, S. F.; Solov'ev, K. N.; Kachura, T. F.; Arabei, S. A.; Skakovskii, E. D. Interpretation of the Soret Band of Porphyrins Based on the Polarization Spectrum of N-methyltetraphenylporphin Fluorescence. *J. Appl. Spectrosc.* **1999**, *66*, 68−75.
(32) Nesset, M. J. M.; Shokhirev, N. V.; Enemark, P. D.; Jacobson, S. E.; Walker, F. A. Models of the Cytochromes. Redox Properties and Thermodynamic Stabilities of Complexes of "hindered" Iron(III) and Iron(II) Tetraphenylporphyrinates with Substituted Pyridines and Imidazoles. *Inorg. Chem.* **1996**, *35*, 5188−5200.
(33) Hunger, J.; Stoppa, A.; Thoman, A.; Walther, M.; Buchner, R. Broadband Dielectric Response of Dichloromethane. *Chem. Phys. Lett.* **2009**, *471*, 85−91.
(34) Stewart, J. J. P. Optimization Parameters for Semiempirical Methods. 1. Method. *J. Comput. Chem.* **1989**, *10*, 209−220.
(35) Stewart, J. J. P. Optimization Parameters for Semiempirical Methods. 2. Applications. *J. Comput. Chem.* **1989**, *10*, 221−264.
(36) Nicholson, R. S.; Shain, I. Theory of Stationary Electrode Polarography. Single Scan and Cyclic Methods Applied to Reversible, Irreversible, and Kinetic Systems. *Anal. Chem.* **1964**, *36*, 706−723.
(37) Ragan, C. I.; Reed, J. S. Regulation of Electron Transfer by Quinone Pool. *J. Bioener. Biomembr.* **1986**, *18*, 403−418.
(38) Wood, P. M. The Potential Diagram for Oxygen at pH 7. *Biochem. J.* **1988**, *253*, 287−289.
(39) McCandlish, E.; Miksztal, A. R.; Nappa, M.; Sprenger, A. Q.; Valentine, J. S.; Stong, J. D.; Spiro, T. G. Reactions of Superoxide with Iron Porphyrins in Aprotic Solvents. A High Spin Ferric Porphyrin Peroxo Complex. *J. Am. Chem. Soc.* **1980**, *102*, 4268−4271.
(40) Shirono, K.; Morimatsu, T.; Takemura, F. Gas Solubilities (CO_2, O_2, Ar, N_2, H_2, and He) in Liquid Chlorinated Methanes. *J. Chem. Eng. Data* **2008**, *53*, 1867−1871.
(41) Bielski, B. H. J.; Cabelli, D. E.; Arudi, R. L.; Ross, A. B. Reactivity of HO_2/O_2^- Radicals in Aqueous Solution. *J. Phys. Chem. Ref. Data* **1985**, *14*, 1041−1100.
(42) More, K. M.; Eaton, G. R.; Eaton, S. S. Effect of a Single Ortho Substituent on the Rate of Dimerization of Iron(III) Tetraphenylporphyrin Hydroxides. *Inorg. Chem.* **1985**, *24*, 3698−3702.
(43) Langmuir, I. The Adsorption of Gases on Plane Surfaces of Glass, Mica and Platinum. *J. Am. Chem. Soc.* **1918**, *40*, 1361−1403.
(44) Sparnaay, M. J. Physisorption on Heterogeneous Surfaces. *Surf. Sci.* **1968**, *9*, 100−118.
(45) Schmidt, T. J.; Paulus, U. A.; Gasteiger, H. A.; Behm, R. J. The Oxygen Reduction Reaction on a Pt/Carbon Fuel Cell Catalyst in the Presence of Chloride Anions. *J. Electroanal. Chem.* **2001**, *508*, 41−47.
(46) Jaouen, F.; Dodelet, J.-P. O_2 Reduction Mechanism on Non-Noble Metal Catalysts for PEM Fuel Cells. Part I: Experimental Rates of O_2 Electroreduction, H_2O_2 Electroreduction, and H_2O_2 Disproportionation. *J. Phys. Chem. C* **2009**, *113*, 15422−15432.
(47) Elbaz, L.; Korin, E.; Soifer, L.; Bettelheim, A. Evidence for the Formation of Cobalt Porphyrin-Quinone Complexes Stabilized at Carbon-Based Surfaces Toward the Design of Efficient Non-Noble-Metal Oxygen Reduction Catalysts. *J. Phys. Chem. Lett.* **2010**, *1*, 398−401.
(48) Elbaz, L.; Korin, E.; Soifer, L.; Bettelheim, A. Electrocatalytic Oxygen Reduction by Co(III) Porphyrins Incorporated in Aerogel Carbon Electrodes. *J. Electroanal. Chem.* **2008**, *621*, 91−96.
(49) Elbaz, L.; Korin, E.; Soifer, L.; Bettelheim, A. Mediation at High Potentials for the Reduction of Oxygen to Water by Cobalt Porphyrin-Quinone Systems in Porous Aerogel Carbon Electrodes. *J. Electrochem. Soc.* **2010**, *157*, B27−B31.
(50) Hieringer, W.; Flechtner, K.; Kretschmann, A.; Seufert, K.; Auwärter, W.; Barth, J. V.; Görling, A.; Steinrück, H.-P.; Gottfried, J. M. The Surface Trans Effect: Influence of Axial Ligands on the Surface Chemical Bonds of Adsorbed Metalloporphyrins. *J. Am. Chem. Soc.* **2011**, *133*, 6206−6222.